Research Article | Vol. 28, No. 19 / 14 September 2020 / Optics Express 27532
Optics EXPRESS

Multi-objective collaborative optimization strategy for efficiency and chromaticity of stratified OLEDs based on an optical simulation method and sensitivity analysis

XIANHUA KE,[1] HONGGANG GU,[1,2] LINYA CHEN,[1] XUENAN ZHAO,[1] JIAOJIAO TIAN,[1] YATING SHI,[1] XIUGUO CHEN,[1] CHUANWEI ZHANG,[1] HAO JIANG,[1] AND SHIYUAN LIU[1,3]

[1] *State Key Laboratory of Digital Manufacturing Equipment and Technology, Huazhong University of Science and Technology, Wuhan, Hubei 430074, China*
[2] *hongganggu@hust.edu.cn*
[3] *shyliu@hust.edu.cn*

Abstract: The low efficiency and dissatisfactory chromaticity remain as important challenges on the road to the OLED commercialization. In this paper, we propose a multi-objective collaborative optimization strategy to simultaneously improve the efficiency and ameliorate the chromaticity of the stratified OLED devices. Based on the formulations derived for the current efficiency and the chromaticity Commission International de L'Eclairage (CIE) of OLEDs, an optical sensitivity model is presented to quantitatively analyze the influence of the layer thickness on the current efficiency and the CIE. Subsequently, an evaluation function is defined to effectively balance the current efficiency as well as the CIE, and a collaborative optimization strategy is further proposed to simultaneously improve both of them. Simulations are comprehensively performed on a typical top-emitting blue OLED to demonstrate the necessity and the effectivity of the proposed strategy. The influences of the layer thickness incorporated in the blue OLED are ranked based on the sensitivity analysis method, and by optimizing the relative sensitive layer thicknesses in the optical views, a 16% improvement can be achieved for the current efficiency of the OLED with desired CIE meantime. Hence, the proposed multi-objective collaborative optimization strategy can be well applied to design high-performance OLED devices by improving the efficiency without chromaticity quality degradation.

1. Introduction

Organic light emitting diodes (OLEDs) currently have gained considerable attentions as one of the emerging displays and solid-state lighting technologies [1–3]. One of the key issues for high-quality OLED devices is to improve the optical characteristics of micro-cavity OLED [4–7]. Various output optical emission characteristics, including efficiency and chromaticity, are determined by the micro-cavity effect, which is resulted by the optical interference within stratified layers and can be tuned by changing the layer thicknesses in OLEDs [8–10]. Optical modeling of stratified OLED devices, as one way to alleviate the repeated trial cost, has played an important role in designing the OLED layer structures by optimizing the micro-cavity effect [11–14].

Due to the total internal reflection between the layer interfaces, lights generated from the emitting materials will be coupled into different optical modes, such as air emission mode, substrate mode, waveguide mode, and surface plasmon polariton mode [15–17]. In order to enhance the moderate efficiency of the OLED, various techniques, including layer thickness tuning techniques [18–21], periodicity patterns [22–24] and photonic crystals [25–28], have been

#398998 https://doi.org/10.1364/OE.398998
Journal © 2020 Received 29 May 2020; revised 3 Aug 2020; accepted 26 Aug 2020; published 2 Sep 2020

Optics EXPRESS

widely employed to extract light trapped in the micro-cavity structures. Significant achievements have been made in the efficiency enhancement of stratified OLED. However, in addition to the moderate efficiency, the dissatisfactory chromaticity remains as another major challenge on the commercialization road of OLEDs [3,29]. The studies mentioned are almost emphasis on the efficiency enhancement, while so far pay less attention on the chromaticity amelioration of the OLEDs. Thus, it is highly desirable for methodologies to simultaneously improve the efficiency as well as the chromaticity of stratified OLED devices.

The working principle of OLEDs can be briefly described as follows: the injected hole-electron pair formed in the emitting layer radiates in the stratified layer system. From the optical point of view, the emissive performances of the stratified OLEDs, including the efficiency and chromaticity, are greatly dependent on the optical properties of the emitter and the micro-cavity structures. Thus, investigating proper emitters or host materials [30–33], and tuning the micro-cavity effect can be conducive to improve the emissive performances [14,34]. Whereas to the best of our knowledge, it is rarely reported to simultaneously analyze and optimize the efficiency as well as chromaticity by tuning the micro-cavity effect of OLED.

In this work, we propose a multi-objective collaborative optimization strategy for the stratified OLEDs to simultaneously improve the efficiency and the chromaticity. Considering that the anisotropic materials are widely used in the OLED structure [35–37], optical formulations are firstly derived for the current efficiency and the chromaticity Commission International de L'Eclairage (CIE) coordinates of stratified anisotropic OLED devices. Then sensitivity model is presented to evaluate the influence of the layer thickness on current efficiency and CIE of OLED. Finally, by changing the layer thicknesses to tune the micro-cavity effect, a collaborative optimization strategy is proposed to improve the current efficiency of the OLED device but without chromaticity quality degradation meantime.

2. Theory

2.1. Optical formulations for stratified anisotropic OLEDs

Various output emission characteristics, such as current efficiency and CIE, are affected by the micro-cavity effect, which can be well tuned by changing the OLED layer thickness. In order to obtain high-performance OLED devices, optical formulations for the influence of the micro-cavity on the emission characteristics are a prerequisite to successfully optimize the efficiency and chromaticity.

The underlying principle of light generation mechanism in OLEDs can be described as the radiative decay of molecular excited states, namely excitons. According to the well-known Chance, Prock, and Sibley (CPS) theory [38–40], the exciton decay emission described in quantum-mechanical approach is equivalent to the radiation of an electric dipole antenna expressed in classical electromagnetic approach. Therefore, the exciton emission in OLED device can be simplified as the dipole radiation in a microcavity, as shown in Fig. 1.

The optical properties of the l-th film layer can be characterized by the thickness d_l and the dielectric tensor $\boldsymbol{\varepsilon}_l$ of the material. The subscript 's' in Fig. 1 denotes the layer index of the dipole layer in the stratified OLED device. The dielectric tensor $\boldsymbol{\varepsilon}$ of the layer material with optical anisotropy properties can be described by two dielectric eigenvalues: ε_{h} and ε_{v}. These eigenvalues are related to the optical constants (i.e., the refractive indices n and the extinction coefficients k), and they can be given by

$$\varepsilon_{\mathrm{h}} = (n_{\mathrm{o}} + \mathrm{j}k_{\mathrm{o}})^2, \tag{1a}$$

$$\varepsilon_{\mathrm{v}} = (n_{\mathrm{e}} + \mathrm{j}k_{\mathrm{e}})^2, \tag{1b}$$

Optics EXPRESS

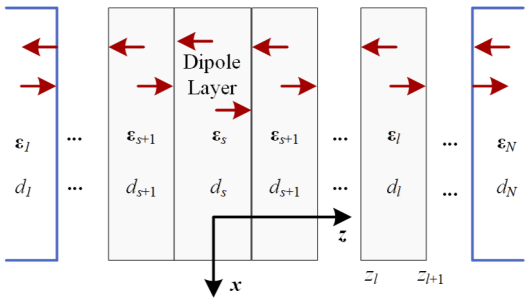

Fig. 1. Simplified formulation model for the stratified anisotropic OLED structure with dipole in the s-th layer (dipole layer). Each layer is characterized by thickness d and dielectric tensor $\boldsymbol{\varepsilon}$.

where j is the imaginary unit, subscripts 'h' and 'v' indicate the directions parallel to and perpendicular to the interface respectively, n_o and k_o correspond to ordinary optical constants while n_e and k_e correspond to extraordinary optical constants.

According to Purcell effect [17,41,42], the spontaneous decay rate of the dipole as well as the radiation power could be modified by the optical environment, as described by

$$F = \frac{\Gamma_r^*}{\Gamma_r} = \frac{P}{P_0}. \tag{2}$$

Here, Γ_r is the intrinsic radiative decay rate of the excited state while Γ^*_r is the real radiative decay rate which modified by the optical environment. F is the Purcell factor, P and P_0 are the total emissive power of an oscillating electric dipole in the OLED structures and in infinite emitting materials respectively. The optical power P radiated by dipole within the multilayer systems can be calculated using the superposition of plane and evanescent waves method [43–45]. Therefore, the Purcell factor of the dipole antenna in the microcavity structures can be written as an integral

$$F = \int_0^\infty K(u)\mathrm{d}u = \int_0^\infty [\Theta \cdot K_s^{\mathrm{TM,v}} + (1-\Theta)\cdot(K_s^{\mathrm{TE,h}} + K_s^{\mathrm{TM,h}})]\mathrm{d}u, \tag{3}$$

where u is the normalized in-plane wavevector, subscripts 'h' and 'v' denote the special cases that the orientated dipole is parallel and perpendicular to the interface, namely the horizontal oriented dipole and the vertical oriented dipole, respectively. The orientation parameters Θ here describes the proportion of the vertical orientated dipole. The superscript 'TM' and 'TE' indicate the transverse magnetic wave and the transverse electric wave, respectively. K(u) is the power dissipation function depending on the in-plane wavevector u, and can be detailed as [43]

$$K_s^{\mathrm{TM,v}} = \frac{3}{4}\mathrm{Re}\left[\frac{u^3}{\sqrt{1-u^2}}(A'_s - A_s)(A_s + A'_s)^*\right], \tag{4a}$$

$$K_s^{\mathrm{TE,v}} = 0 \tag{4b}$$

$$K_s^{\mathrm{TE,h}} = \frac{1}{2}\left(\frac{3\sqrt{\varepsilon_{s,\mathrm{h}}}}{3\varepsilon_{s,\mathrm{h}} + \varepsilon_{s,\mathrm{v}}}\right)\mathrm{Re}\left[\frac{u\sqrt{\varepsilon_{s,\mathrm{v}}}}{\sqrt{\varepsilon_{s,\mathrm{h}}/\varepsilon_{s,\mathrm{v}} - u^2}}(C_s + C'_s)(C'_s - C_s)^*\right], \tag{4c}$$

$$K_s^{\mathrm{TM,h}} = \frac{1}{2}\mathrm{Re}\left[\frac{3u\varepsilon_{s,\mathrm{v}}\sqrt{1-u^2}}{3\varepsilon_{s,\mathrm{h}} + \varepsilon_{s,\mathrm{v}}}(B'_s - B_s)(B_s + B'_s)^*\right]. \tag{4d}$$

Here, the symbol Re[·] indicates the real part, the coefficients A'_s, B'_s, C'_s and A_s, B_s, C_s correspond to the forward and backward traveling waves in the dipole layer respectively, and $\varepsilon_{s,\mathrm{h}}$

Optics EXPRESS

and $\varepsilon_{s,\mathrm{v}}$ are the dielectric eigenvalues of the dipole layer material. Similarity, the power P_{out} emitting into the air and the corresponding F_{out} can be written as

$$\frac{P_{\mathrm{out}}}{P_0} = F_{\mathrm{out}} = \int_0^{k_0/k_s} K_{\mathrm{out}}(u)\mathrm{d}u = \int_0^{k_0/k_s} [\Theta \cdot K_{\mathrm{out}}^{\mathrm{TM},z} + (1-\Theta)\cdot(K_{\mathrm{out}}^{\mathrm{TE},x} + K_{\mathrm{out}}^{\mathrm{TM},x})]\mathrm{d}u. \quad (5)$$

Here, k_0 and k_s are the amplitude of the wavevector in the air and in dipole layer respectively. K_{out} is the power density per unit du in the outmost layer (usually denotes the air layer).

In real OLED devices within the electroluminescence process considered, the emissive excitons can be treated as an ensemble of incoherent dipole radiators. Therefore, the output emissive spectrum of the stratified OLED structures can be easily obtained by an incoherent superposition of all contributions as [46]

$$P_{\mathrm{out}}(\lambda) = (I_{\mathrm{inj}}/e)\cdot\gamma\cdot\eta_{S/T}\cdot q_{\mathrm{eff}}\cdot S(\lambda)\int_z g(z)\frac{F_{\mathrm{out}}}{F}dz. \quad (6)$$

Here, λ is the wavelength, $S(\lambda)$ is the internal electroluminescence spectrum of the emitting material, I_{inj} denotes the current injected into the OLED device and e denotes the elementary charge, γ is the probability of charge carrier recombination and subsequent exciton formation, $\eta_{\mathrm{S/T}}$ is the singlet/triplet factor describing the allowed excited states according to the spin statistics. Since charge carriers are usually homogeneously distributed in the plane of the layered system interfaces, the spatial distribution of excitons in the OLED active layer can be simplified to a one-dimensional emission zone function $g(z)$, which depends solely on the z. The effective radiative quantum efficiency q_{eff} is derived from the intrinsic radiative quantum efficiency q and can be defined as

$$q_{\mathrm{eff}} = \frac{\Gamma_r^*}{\Gamma_r^*+\Gamma_{nr}} = \frac{F\Gamma_r}{F\Gamma_r+\Gamma_{nr}} = \frac{q}{1-q+qF}. \quad (7)$$

Based on the emissive spectrum formulation defined in Eq. (6), the current efficiency η_{CE} of the OLED can be calculated as

$$\eta_{\mathrm{CE}} = 683\frac{1}{I_{\mathrm{inj}}}\int_{380}^{780} P_{\mathrm{out}}(\lambda)Y(\lambda)d\lambda, \quad (8)$$

where $Y(\lambda)$ is the standardized photopic luminosity function which represents the response of a typical human eye under bright conditions [47]. Based on the output emissive spectrum, The chromaticity CIE 1931 coordinates [48] can also be easily calculated with respect to the CIE standard observers x_i as following

$$X_i = \frac{\int_{380}^{780} P_{\mathrm{out}}(\lambda)x_i(\lambda)d\lambda}{\sum_{i=1}^{3}\int_{380}^{780} P_{\mathrm{out}}(\lambda)x_i(\lambda)d\lambda}. \quad (9)$$

Here the x_i is the i-th color matching function for CIE 1931 color space, which indicates the color of OLED display or light source. Equations (8) and (9) are the derived formulations for the current efficiency and the CIE coordinates of OLED structures. Thereby, based on the proposed formulations, optical analysis and optimization can be performed on the current efficiency as well as the CIE coordinates.

2.2. Optical sensitivity model for stratified OLEDs

The systematic analysis for the influence of the layer thickness on the current efficiency and CIE can be conductive to improve these performances of the OLED devices. Hence, an optical

Optics EXPRESS

sensitivity model is presented here to comprehensively analyze the effects of the OLED layer thickness.

Based on the formulations derived for stratified OLED devices, the current efficiency and the CIE coordination can be further re-formulated as

$$\eta_{\mathrm{CE}}(\mathbf{d}) = \eta_{\mathrm{CE}}(\Theta, g(z), q, \mathbf{d}, \boldsymbol{\varepsilon}), \tag{10a}$$

$$X_i(\mathbf{d}) = X_i(\Theta, g(z), q, \mathbf{d}, \boldsymbol{\varepsilon}). \tag{10b}$$

Herein, the dipole orientation Θ, dipole distribution $g(z)$ and intrinsic quantum efficiency q are relative to the emitter properties, while the layer thickness $\mathbf{d}$ and the dielectric tensor $\boldsymbol{\varepsilon}$ are relative to the micro-cavity properties of the OLED layer system. Since in the optimization process of certain OLED devices by tuning the micro-cavity effect, the parameters Θ, $g(z)$, q and $\boldsymbol{\varepsilon}$ are usually assumed to be constants, then the mentioned formulations of OLED can be simplified as an optical model depending solely on the layer thicknesses $\mathbf{d}$.

In the optical model of the stratified OLED devices, the input is the layer thickness, and the outputs are the OLED emission characteristics, including the current efficiency and the CIE. Sensitivity analysis allows the identification of the input parameters that have the greatest influence on the model output, it consequently provides useful insight into which input parameters (i.e. the layer thickness) contributes most to the variability of the model output (i.e. the current efficiency and CIE of the OLED devices). In general, there are two types of sensitivity analysis: local and global [49]. The local sensitivity analysis evaluates changes in the current efficiency as well as CIE with respect to variations in thickness of a single layer. While in a global sensitivity analysis, all the layer thicknesses are varied simultaneously over the entire feasible domain, thus allows to evaluate the relative effect of each individual layer thickness as well as the interactions between different layer thicknesses.

In order to facilitate sensitivity analysis, the optical model can be linearly transformed to be relative quantities as following

$$y_1(\mathbf{d}) = \frac{\eta_{\mathrm{CE}}(\mathbf{d}) - \eta_{\mathrm{CE}}(\mathbf{d}_0)}{\eta_{\mathrm{CE}}(\mathbf{d}_0)}, \tag{11}$$

$$y_2(\mathbf{d}) = \frac{X_i(\mathbf{d}) - X_{i,0}}{X_{i,0}}, \tag{12}$$

where $\mathbf{d}_0$ is a thickness vector corresponding to the original OLED micro-cavity structure, $X_{i,0}$ is the i-th desired CIE coordinate. Then the local sensitivity index L_i which describes the effect of the OLED layer thickness can be defined as

$$L_i = [y(d_1, d_2, \cdots, d_{i-1}, d_i + \delta d_i, d_{i+1}, d_N) - y(\mathbf{d})]/\delta d_i. \tag{13}$$

Here, the δd_i is the variations of the i-th layer thickness d_i, and thickness of the other layers would remain unchanged. Based on the Morris method [50], the global sensitivity can be approximated by averaging the local sensitivity indices at multiple random structures within the layer thickness domain. Therefore, the global sensitivity index μ_i of the i-th layer can be obtained as

$$\mu_i = \sum_{j=1}^{r} \frac{L_{i,j}}{r}, \tag{14}$$

where, the $L_{i,j}$ is the calculated j-th local sensitivity index for the i-th layer thickness. r is the number of the samples for different random OLED structures.

Optics EXPRESS

2.3. Multi-objective optimization strategy for stratified OLEDs

To balance the efficiency and the chromaticity of stratified OLED devices, a collaborative optimization strategy is proposed here to simultaneously improve the current efficiency and the CIE coordinates. The optimal problem can be firstly re-formulated as

$$\begin{aligned} \mathbf{d}^* &= \arg\max_{\mathbf{d}\in\Omega} \eta_{\mathrm{CE}}(\mathbf{d}) \\ s.t.\ \ & X_i(\mathbf{d}) \in \Delta_i. \end{aligned} \tag{15}$$

Herein, $\mathbf{d}^*$ is the optimal thickness corresponding to high-performance OLED devices. Ω and Δ_i respectively denote the acceptable domain for layer thickness and CIE X_i coordinate. The Lagrange multiplier method and penalty function method are usually applied to deal with this optimal problem with inequality constraints [51]. The kernel of the mentioned methods is to turn the constrained optimization problem into an unconstrained optimization problem, however, it is often difficult to determine the multipliers in the Lagrange method and the weighting factors in the penalty function. To avoid this limitation, a single-valued function $f(\mathbf{d})$ is proposed here to remove constraints to be an unconstrained form as

$$\mathbf{d}^* = \arg\max_{\mathbf{d}\in\Omega} f(\mathbf{d}), \tag{16}$$

where the evaluation function $f(\mathbf{d})$ describes the overall performance, including the current efficiency and the CIE, of the OLED devices at the design stage. Naturally, the evaluation function $f(\mathbf{d})$ can be defined as a product of two functions which correspond to the current efficiency and the CIE coordinates respectively. The formulation can be written as [52]

$$f(\mathbf{d}) = f_1(\mathbf{d}) \cdot f_2(\mathbf{d}), \tag{17}$$

where the functions $f_1(\mathbf{d})$ and $f_2(\mathbf{d})$ are defined as

$$f_1(\mathbf{d}) = \frac{\eta_{\mathrm{CE}}(\mathbf{d})}{\eta_{\mathrm{CE}}(\mathbf{d}_0)}, \tag{18a}$$

$$f_2(\mathbf{d}) = \prod_{i=1}^{2} \exp\left(-\left\|\frac{X_i(\mathbf{d}) - X_{i,0}}{\delta\Delta_i}\right\|\right). \tag{18b}$$

Herein, the symbol $||\cdot||$ denotes the second norm, the symbol Π denotes the multiplication operator, and $\delta\Delta_i$ is the acceptable deviation domain for the i-th CIE coordinate. Function $f_1(\mathbf{d})$ obviously describes the η_{CE} enhancement ratios of the OLED structure with layer thickness $\mathbf{d}$ to the original OLED structure with layer thickness $\mathbf{d}_0$. While function $f_2(\mathbf{d})$ expresses the punishment factor caused by relative deviation of the desired CIE coordinates. Therefore, the constrained formulation in Eq. (15) to simultaneously improve both the current efficiency and the CIE is turned into an unconstrained optimization problem, which can be easily solved by the common iterative algorithm, such as Newton method and conjugate gradient method [51].

In order to better illustrate the effect of the function $f_2(\mathbf{d})$, an example curve of f_2 is given in Fig. 2. In this situation, the desired CIE coordinate X_2 is assumed as $X_{2,0} = 0.055$, and its acceptable deviation scope is set as $\delta\Delta_2 = 0.004$ with the acceptable domain $\Delta_2 = [0.053, 0.057]$. The function is $f_2 = 0.6$ at the boundary, namely $X_2 = 0.053$ and $X_2 = 0.057$, of the domain, and reach the peak $f_2 = 1$ at $X_2 = X_{2,0} = 0.055$. It can be easily observed that this function can well be applied to limit the CIE coordinate X_2 within the acceptable domain Δ_2.

Optics EXPRESS

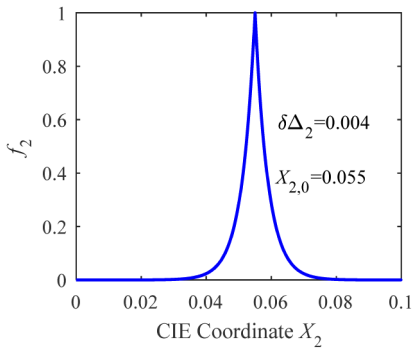

Fig. 2. An example curve of the function f_2 to constrain the CIE.

3. Results

The OLED devices based on red and green phosphorescent iridium complexes are recently successfully commercialized, while those blue ones still suffer the relatively low current efficiency and the dissatisfactory CIE coordinates. Therefore, here we will focus on the blue OLED devices in the following optical analysis and optimization.

A typical top-emitting blue OLED device and corresponding intrinsic emitter spectrum of the emitting material are shown in Fig. 3. The OLED structure can be described as: Capping layer (CPL, 85 nm) /Cathode (13 nm)/ Electron transport layer (ETL, 30 nm)/ Hole block layer (HBL, 5 nm)/ Emitting layer (EML, 20 nm)/ Hole injection layer (Functional layer for blue emitting layer, FLB (5 nm) /Hole transport layer (HTL, 125 nm) /Hole injection layer (HIL, 10 nm) / Anode (Indium Tin Oxide, ITO, 15 nm) /Ag (140 nm). The EML layer is the emitting (dipole) layer, and the radiative dipoles are all assumed to be located at 2 nm away from the FLB layer interface, namely $g(z) = \delta(0.9)$ in Eq. (6). The current I_{inj} applied to the OLED device is 10 mA/cm^2, while parameters γ and $\eta_{\text{S/T}}$ in Eq. (6) are assumed to be 1 and 0.25 respectively. The intrinsic quantum radiation efficiency q of the emitting material is 0.75, and the dipoles are random orientated, namely $\Theta = 1/3$. The peak wavelength of the intrinsic emitter spectrum is at 460 nm with half peak width corresponding to 40 nm. It should be noted that the optical simulations are all performed by the custom-made MATLAB codes. And it is also worth to pointing out that for this top-emitting blue OLED device, the CIE 1931 y coordinate denoted by X_2 usually attract more attentions than the others, and the desired value is assumed to be $X_{2,0} = 0.055$, with the acceptable domain $\Delta_2 = [0.053, 0.057]$. Hence based on the demand of this top-emitting blue OLED, the requirement is to achieve the highest possible current efficiency η_{CE} and keep the CIE 1931 y coordinate (X_2) at the desired value meantime.

The optical constants including the refractive indices n and extinction coefficient k for materials incorporated in the OLED can be determined by a spectroscopic ellipsometer (ME-L, Wuhan Eoptics Technology Co.) [53,54]. The detailed spectroscopic information is obtained separately for each film layer, which is prepared on a substrate by the same process as the device multilayer sequence. The optical constants of the anisotropic layer, the metal layer and the organic layers are respectively shown in Figs. 4 (a)–(c) in the visible band. The precision of the optical constant (n & k) is sample dependent, generally, the derivation of the optical constant is about 0.005. From Fig. 4(a) we found that the refractive index of the CPL material shows strong negative optical anisotropy. Based on the optical micro-cavity properties of the top-emitting blue OLED and the derived formulations in Eqs. (8) and (9), the current efficiency η_{CE} and CIE 1931 coordinate X_2 can be calculated and investigated. Then we can easily perform optical analysis and optimization

Optics EXPRESS

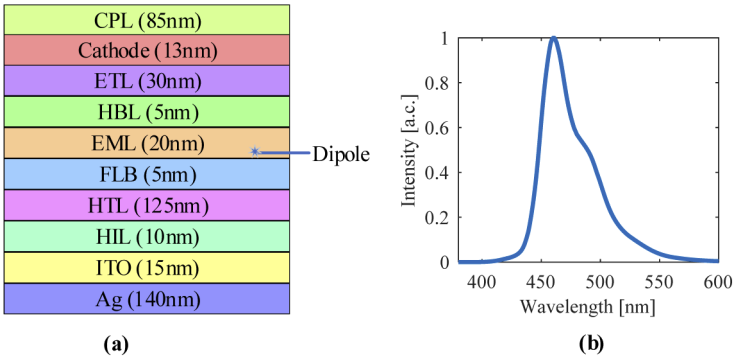

Fig. 3. (a). Structures of a top-emitting blue OLED. The distribution of the dipoles is assumed to be $g(z) = \delta(0.9)$, which means that all dipoles are located in the EML layer with 2 nm away from the FLB layer interface; (b) Intrinsic luminescence spectrum of the emitting material with a peak wavelength 460 nm and 40 nm half peak width.

on these OLED output emissive characteristics through micro-cavity tuning by changing the multilayer thicknesses.

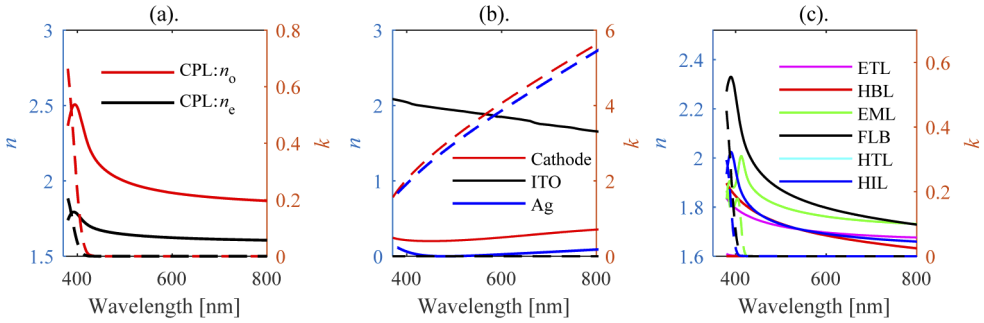

Fig. 4. Optical constants of the materials incorporated in the OLED in the visible band: (a) anisotropic layer CPL; (b) metal layers; (c) organic layers. It can be observed that the CPL layer shows strong negative optical anisotropic since $n_o > n_e$.

The systematic analysis of the influence of the layer thickness on the current efficiency and CIE can be conductive to design high-performance OLED devices. The local sensitivity analysis of the current efficiency η_{CE} and CIE X_2 are investigated and shown in Fig. 5. During the local sensitivity analysis of a single layer incorporated in the OLED structure, the thicknesses of the other layers are kept as the same as shown in Fig. 3(a). The results using our model are denoted by solid lines, while the results using the commercial software SETFOS [55] are denoted by open circles as a comparison. The high agreement between the results of our model and SETFOS verify the correctness of our proposed formulations. From Fig. 5(a) we found that the η_{CE} can reach the peak at the layer thickness near 50 or 150 nm, however, it can be obviously observed from Fig. 5(b) that the CIE X_2 is dissatisfactory for the blue OLED at these thickness configurations. These results indicate that under the design configuration with layer thicknesses corresponding to the optimal η_{CE}, the CIE X_2 is most likely not satisfactory, namely the efficiency and the desired chromaticity coordinates are in contradiction with each other in some sense. Therefore, in the practical design of a high-performance OLED structure, we need to balance the efficiency and the chromaticity.

Optics EXPRESS

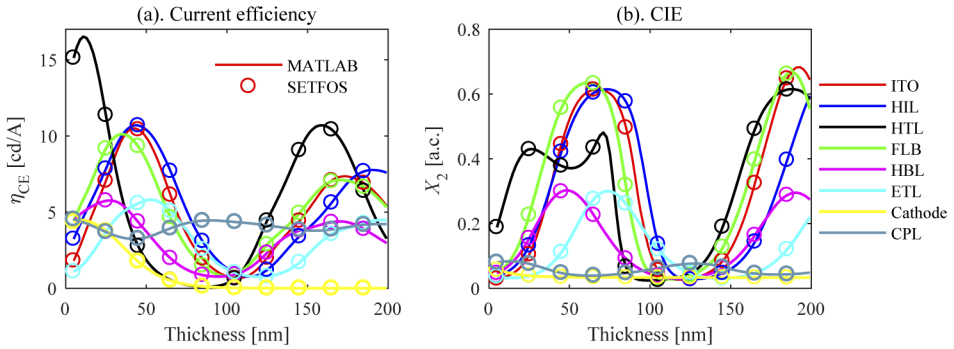

Fig. 5. Performance curves of the top-emitting blue OLED device versus the layer thicknesses: (a) current efficiency η_{CE} vs thickness; (b) CIE X_2 vs thickness. Results by our model denoted by solid lines are compared with results by the commercial software Fluxim SETFOS denoted by open circles.

The main limitation of the local sensitivity analysis is that it evaluates the current efficiency and CIE with respect to variation in only one layer thickness at a time, hence it does not allow for the evaluation of simultaneous changes in all the layer thickness of OLED devices. Therefore, the global sensitivity analysis should be applied to carry the interaction between different layer thicknesses, and further evaluate the influence of the OLED layer thickness on the mentioned characteristics.

Given that the layer thickness can span a wide range for the OLED optical model, global sensitivity analysis is an innovative approach for determining which one layer contribute most to the optical behavior of the OLED system. Based on the sensitivity model proposed, global sensitivity analysis is performed for the thickness of all layers incorporated in the blue OLED stack, and the normalized results of layer thickness within Ω are shown in Fig. 6. As stated in Eq. (15), the parameter Ω denotes that all the layer thicknesses are changed within domain Ω. From Fig. 5 we can find that the η_{CE} almost can reach its first peak at layer thicknesses within 50 nm, hence results of layer thickness within $\Omega = [0, 50]$ are shown in Fig. 6(a). In addition, sometimes only minor variations of the layer structure are expected during the design process, as a consequence, results of layer thickness within $\Omega = [\mathbf{d}_0-5, \mathbf{d}_0+5]$ are also shown in Fig. 6(b). The label of the x-axis in the figure corresponds to the layer indices, i.e. L_1–L_{10} denote the layer Ag, ITO, HIL, HTL, FLB, EML, HBL, ETL, Cathode, and CPL. The layer Ag is not analyzed here because this film is usually very thick. It can be obviously observed from Fig. 6 that, compared with the current efficiency and CIE of the OLED, the proposed evaluation function $f(\mathbf{d})$ can well distinguish the influence of the layer thickness, and meanwhile balance both the current efficiency and CIE. Besides, we can find from Fig. 6 that function $f(\mathbf{d})$ is more sensitive to the thicknesses of the L_2 (ITO), L_3 (HIL), L_5 (FLB), L_9 (Cathode) layer. Therefore, in this work, the optical optimization will be focused on these concerned layers to improve the performances of the top-emitting blue OLED.

The independent influences of the concerned OLED layer thicknesses on the evaluation function $f(\mathbf{d})$ are elaborated in Fig. 7. Sharp peaks can be obviously observed in these curves, and the layer thickness configurations corresponding to these peaks indicate excellent CIE coordinate X_2. These designed structure configurations and the relevant optical performances are all shown in cases C1 to C4 as listed in Table 1. The cases C1 to C4 correspond to the peak thickness $d_{ITO} = 17$ nm, $d_{HIL} = 13$ nm, $d_{FLB} = 7$ nm and $d_{Cathode} = 7$ nm, respectively. For comparison, the performances of the original OLED structure shown in Fig. 3 are also listed as case C0 in Table 1. The results show that significant amelioration has been achieved for the CIE coordinate.

Optics EXPRESS

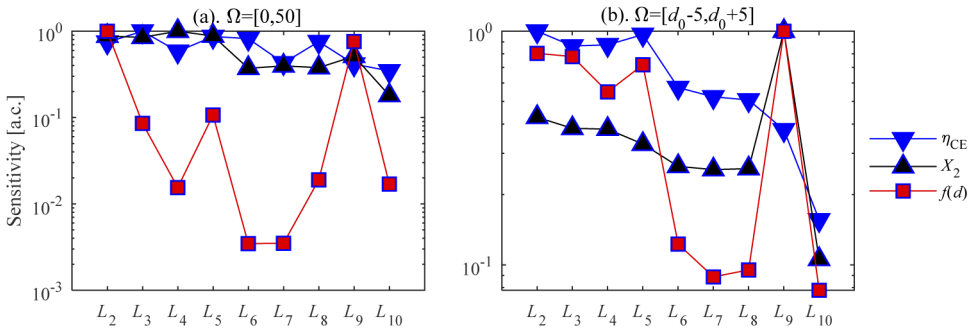

Fig. 6. Global sensitivity analysis results of the layer incorporated in the blue OLED stack: (a) layer thicknesses are within $\Omega = [0, 50]$; (b) layer thicknesses are within $\Omega = [\mathbf{d}_0-5, \mathbf{d}_0+5]$.

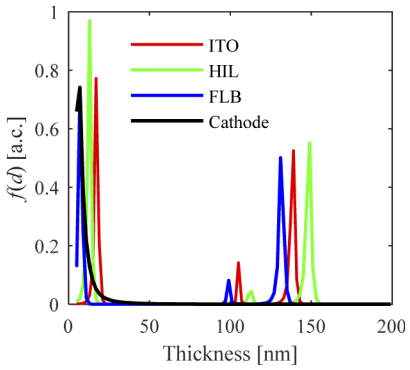

Fig. 7. Simulation results of objective function vs concerned layer thickness independently.

Table 1. Analysis results of the independent layer

Cases	Layer thickness [nm]				Performance	
	ITO	HIL	FLB	Cathode	η_{CE} [cd/A]	X_2
C0	15	10	5	13	4.43	0.046
C1	17	10	5	13	4.96	0.053
C2	15	13	5	13	5.11	0.054
C3	15	10	7	13	4.93	0.053
C4	15	10	5	7	4.43	0.054

Optics EXPRESS

In order to obtain more improvement on the current efficiency and CIE of the blue OLED, optimization is further performed by combining with all the concerned layer thickness within $\Omega = [0, 50]$. Based on the definition of the evaluation function $f(\mathbf{d})$, the amplitude of the function $f_2(\mathbf{d})$ in the $f(\mathbf{d})$ will not exceed one, hence $\Delta f = f(\mathbf{d}) - 1$ indicates at least an improvement of Δf in the η_{CE} with expected CIE X_2. In practical design of OLED, the target evaluation function value is determined by the expected improvement of the OLED device, i.e., $f(\mathbf{d}) = 1 + \Delta f$. Results of the simultaneous optimization of all the four concerned layers are shown in Fig. 8, and the discrete points in the figure indicate that $f(\mathbf{d}) > 1.14$ can be achieved under the thickness configurations. In order to accomplish this target, i.e. $\Delta f = 14\%$ improvement of the η_{CE} with desired CIE $X_2 = X_{2,0} = 0.055$, we can find from the Fig. 8(a) that, the thicknesses of layer ITO and HTL need to be designed to be negatively correlated. In addition, from Fig. 8(b), Fig. 8(d) and Fig. 8(f) we can find that, the thickness of layer FLB should be less than 10 nm, and from Fig. 8(c), Fig. 8(e), Fig. 8(f) that, the cathode layer should be within the range between 10 nm and 20 nm.

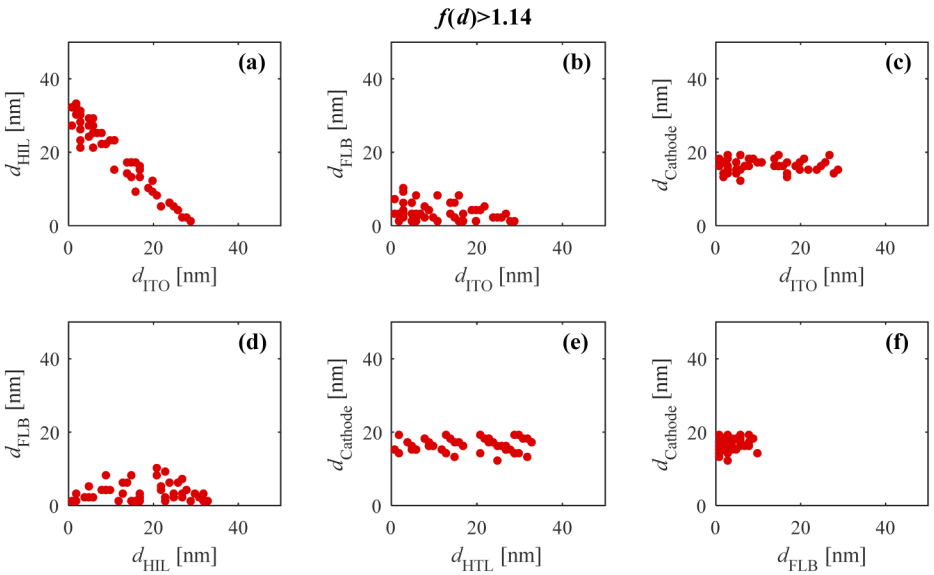

Fig. 8. Optimization results of the layer thicknesses for target $\Delta f = 14\%$ of the blue OLED.

Some outstanding design layer configurations with large evaluation function values are listed as cases C5 to C7 in Table 2. The parameter Δf is also displayed in Table 2 since it could obviously describe the enhanced ratio of the current efficiency η_{CE}. It can be clearly observed from Table 2 that, for all the cases C5 to C7, the current efficiency is significantly improved by at least a 16% and meanwhile the CIE coordinate is well ameliorated for the top-emitting blue OLED device. The spectrums of the original and optimal OLED structures are shown in Fig. 9, herein, the curves of these optimal results from the cases C5 to C7 are completely coincide. Since the goal of the proposed optimization strategy is to simultaneously improve the current efficiency and the CIE of the OLED, layer thicknesses are optimized to tune the microcavity structure to achieve the goal. Compared with the emission spectrum of the initial structure, the spectrum of the optimized device shows an obvious red shift and peak improvement in Fig. 9. The red shift deduced by microcavity effect appears in the spectrum to tune the CIE from $X_2 = 0.046$ to the desired value $X_2 = 0.055$, while the improvement in the peak intensity is to improve the current efficiency. Besides, the results obtained from our model (denoted by solid lines), is compared with the results obtained from SETFOS (denoted by open circles). The high agreement between

Optics EXPRESS

the results of our model and SETFOS further verify the correctness of our proposed formulations. Therefore, the proposed evaluation function and the optimization strategy can be well employed to simultaneously improve the efficiency and the chromaticity of OLED devices.

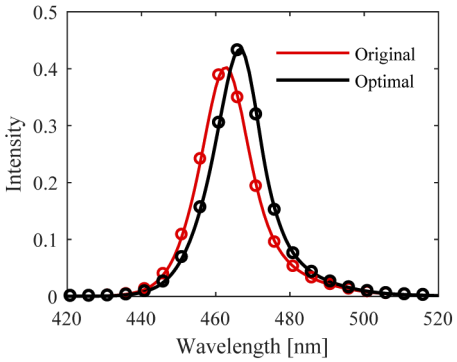

Fig. 9. Spectrum of the original and optimal OLED structure. Results by our model denoted by solid lines are compared with results by the software SETFOS denoted by open circles

Table 2. Collaborative optimization results of the top emitting blue OLED.

Cases	Layer thickness [nm]				Performance		
	ITO	HIL	FLB	Cathode	η_{CE} [cd/A]	X_2	Δf
C5	3	30	3	19	5.160	0.055	16.3%
C6	5	24	6	17	5.152	0.055	16.3%
C7	15	17	2	16	5.176	0.055	16.8%

It is worth noting that, since the proposed optimization strategy is based on tuning the micro-cavity effect by changing the layer thicknesses, the performance improvement of the OLED devices, including the current efficiency and the CIE coordination, usually depends on the initial layer structure and the strength of the microcavity effect. Generally, compared with the bottom-emitting structure, the top-emitting OLEDs (e.g. the OLED device simulated here) contain high reflectively bimetal electrodes, and thus show stronger Purcell effect. Therefore, the effect of the proposed optimization strategy is usually more obvious for top-emitting than the bottom-emitting OLEDs.

4. Conclusion

In this paper, we proposed a multi-objective collaborative optimization strategy for stratified OLED to improve the efficiency and ameliorate the chromaticity. Firstly, a sensitivity model based on Morris method is presented to evaluate the influence of the layer thickness on the current efficiency and the CIE coordinates of the stratified OLED devices. Subsequently, a collaborative optimization strategy, by defining a comprehensive function to balance multiple objects, is reported for the current efficiency improvement and the CIE amelioration. Based on the proposed strategy, we analyzed and optimized the performances of a typical top-emitting blue anisotropic OLED device. We found that the current efficiency and the CIE are likely in contradiction with each other, which highlights the necessity of some tradeoff between the efficiency and the chromaticity in the practical design of OLED structures. Besides, based on the results of the sensitivity analysis, we optimized the thickness of the layers with higher sensitivity to obtain a high-performance blue OLED of a 16% improvement for the current efficiency without CIE degradation. Overall, the proposed collaborative optimization strategy has great potential

Optics EXPRESS

and advantages in the practical design of high-performance OLEDs by simultaneously improving the efficiency and chromaticity of the devices.

Generally, lots of optical emissive characteristics, such as the far-field spectrum and the angular color shift, should also be considered in the optimization design process of the OLED devices in practice. Although here we mainly focus on the optimization of the efficiency and the chromaticity, the proposed collaborative optimization strategy can be well extended to deal with enough characteristics by taking all the parameters into the evaluation function.

Funding

National Natural Science Foundation of China (51525502, 51727809, 51805193, 51975232); Natural Science Foundation of Hubei Province (2018CFA057, 2018CFB559); National Science and Technology Planning Project (2017ZX02101006-004); China Postdoctoral Science Foundation (2016M602288, 2017T100546).

Acknowledgments

The authors thank the technical support from the Experiment Centre for Advanced Manufacturing and Technology in School of Mechanical Science &Engineering of HUST.

Disclosures

The authors declare no conflicts of interest.

References

1. S. Tiwari, M. Singh, S. Mishra, and A. Shrivastava, "Recent Progress in Organic Light-Emitting Diodes," J. Nanoelectron. Optoelectron. **14**(9), 1215–1224 (2019).
2. D. Luo, Q. Chen, B. Liu, and Y. Qiu, "Emergence of Flexible White Organic Light-Emitting Diodes," Polymers **11**(2), 384 (2019).
3. S. Reineke, M. Thomschke, B. Lussem, and K. Leo, "White organic light-emitting diodes: status and perspective," Rev. Mod. Phys. **85**(3), 1245–1293 (2013).
4. Z. H. Wang and S. J. Su, "Molecular and device design strategies for ideal performance white organic light-emitting diodes," Chem. Rec. **19**(8), 1518–1530 (2019).
5. H. Sasabe and J. Kido, "Development of high performance OLEDs for general lighting," J. Mater. Chem. C **1**(9), 1699–1707 (2013).
6. A. Salehi, X. Y. Fu, D. H. Shin, and F. So, "Recent advances in OLED optical design," Adv. Funct. Mater. **29**(15), 1808803 (2019).
7. M. Zhang, Z. Chen, L. Xiao, B. Qu, and Q. Gong, "Optical design for improving optical properties of top-emitting organic light emitting diodes," J. Appl. Phys. **113**(11), 113105 (2013).
8. R. Meerheim, R. Nitsche, and K. Leo, "High-efficiency monochrome organic light emitting diodes employing enhanced microcavities," Appl. Phys. Lett. **93**(4), 043310 (2008).
9. M. Park, Y. Son, G. Kim, R. Lampande, H. Bae, R. Pode, Y. Lee, W. Song, and J. Kwon, "Device performances of third order micro-cavity green top-emitting organic light emitting diodes," Org. Electron. **26**, 458–463 (2015).
10. S. Kwon, E. Lee, K. Kim, H. Choi, M. Park, S. Kim, R. Pode, and J. Kwon, "Efficient micro-cavity top emission OLED with optimized Mg:Ag ratio cathode," Opt. Express **25**(24), 29906–29915 (2017).
11. D. Poitras, C. C. Kuo, and C. Py, "Design of high-contrast OLEDs with microcavity effect," Opt. Express **16**(11), 8003–8015 (2008).
12. S. Yue, R. Guo, Y. Wu, P. Yan, S. Zhang, Z. Zhang, D. Qu, and Y. Zhao, "Optical simulation and optimization of weak-microcavity tandem white organic light-emitting diodes," J. Appl. Phys. **116**(15), 153102 (2014).
13. S. Lee, T. Hoang, J. Lee, and Y. Kim, "Investigation of light out-coupling efficiency of blue OLED using microcavity effects," Phys. B **550**, 122–126 (2018).
14. S. Jeong, S. Jung, H. Kang, S. Choi, S. Hong, J. Lee, K. Yu, N. Kim, S. Kee, D. Lee, and K. Lee, "Controlling the Chromaticity of White Organic Light-Emitting Diodes Using a Microcavity Architecture," Adv. Opt. Mater. **8**(1), 1901365 (2020).
15. R. Meerheim, M. Furno, S. Hofmann, B. Lussem, and K. Leo, "Quantification of energy loss mechanisms in organic light-emitting diodes," Appl. Phys. Lett. **97**(25), 253305 (2010).
16. S. Choi, S. Baek, D. Im, H. Kahng, and H. Kim, "Quantitative modal analysis of optical power flow and energy loss in photonic structures with a dipole emission source," Opt. Express **22**(15), 18499–18512 (2014).

Optics EXPRESS

17. W. Brutting, J. Frischeisen, T. D. Schmidt, B. J. Scholz, and C. Mayr, "Device efficiency of organic light- emitting diodes: progress by improved light outcoupling," Phys. Status Solidi A **210**(1), 44–65 (2013).
18. S. Kim and J. Kim, "Outcoupling efficiency of organic light emitting diodes and the effect of ITO thickness," Org. Electron. **11**(6), 1010–1015 (2010).
19. H. Jeon, B. Pyo, H. Park, S. Park, and M. Suh, "Improved out-coupling efficiency of organic light emitting diodes by manipulation of optical cavity length," Org. Electron. **20**, 49–54 (2015).
20. T. Hoang, S. Lee, J. Lee, Y. Kim, and J. Lee, "Optimum thickness of epsilon negative tri-metal layer electrodes for maximizing OLED outcoupling efficiency," Opt. Express **25**(25), 31006–31016 (2017).
21. A. A. Shcherbakov, A. V. Tishchenko, D. S. Setz, and B. C. Krummacher, "Rigorous S-matrix approach to the modeling of the optical properties of OLEDs," Org. Electron. **12**(4), 654–659 (2011).
22. J. Frischeisen, Q. Niu, A. Abdellah, J. Kinzel, R. Gehlhaar, G. Scarpa, C. Adachi, P. Lugli, and W. Brutting, "Light extraction from surface plasmons and waveguide modes in an organic light-emitting layer by nanoimprinted gratings," Opt. Express **19**(S1), A7–A19 (2011).
23. Y. Bi, J. Feng, Y. Li, Y. Jin, Y. Liu, Q. Chen, and H. Sun, "Enhanced efficiency of organic light-emitting devices with metallic electrodes by integrating periodically corrugated structure," Appl. Phys. Lett. **100**(5), 053304 (2012).
24. D. Hwang, O. Kwon, W. Lee, J. Hong, and T. Kim, "Outcoupling efficiency of organic light-emitting diodes depending on the fill factor and size of the microlens array," Phys. Status Solidi A **211**(8), 1773–1777 (2014).
25. Y. Do, Y. Kim, Y. Song, and Y. Lee, "Enhanced light extraction efficiency from organic light emitting diodes by insertion of a two-dimensional photonic crystal structure," J. Appl. Phys. **96**(12), 7629–7636 (2004).
26. A. Adawi, R. Kullock, J. Turner, C. Vasilev, D. Lidzey, A. Tahraoui, P. Fry, D. Gibson, E. Smith, C. Foden, M. Roberts, F. Qureshi, and N. Athanassopoulou, "Improving the light extraction efficiency of polymeric light emitting diodes using two-dimensional photonic crystals," Org. Electron. **7**(4), 222–228 (2006).
27. H. Fujimoto, M. Yahiro, T. Kawashima, K. Konno, Q. Chen, K. Sawaya, S. Kawakami, and C. Adachi, "Improvement in the light outcoupling efficiency of organic light-emitting diodes using a hemispherical lens and a multipatterned one-dimensional photonic crystal fabricated by autocloning," Appl. Phys. Express **8**(8), 082102 (2015).
28. Y. S. Shim, K. N. Kim, J. H. Hwang, C. H. Park, S. Jung, Y. W. Park, and B. Ju, "Spectral-distortion-free light extraction from organic light-emitting diodes using nanoscale photonic crystal," Nanotechnology **28**(4), 045301 (2017).
29. C. Gather, A. Kohnen, and K. Meerholz, "White organic light-emitting diodes," Adv. Mater. **23**(2), 233–248 (2011).
30. J. Feng, F. Li, W. Gao, S. Liu, Y. Liu, and Y. Wang, "White light emission from exciplex using tris-(8-hydroxyquinoline) aluminum as chromaticity-tuning layer," Appl. Phys. Lett. **78**(25), 3947–3949 (2001).
31. P. Freitag, S. Reineke, S. Olthof, M. Furno, B. Lussem, and K. Leo, "White top-emitting organic light-emitting diodes with forward directed emission and high color quality," Org. Electron. **11**(10), 1676–1682 (2010).
32. X. Li, J. Zhang, Z. Zhao, L. Wang, H. Yang, Q. Chang, N. Jiang, Z. Liu, Z. Bian, W. Liu, Z. Lu, and C. Huang, "Deep Blue Phosphorescent Organic Light-Emitting Diodes with CIEy Value of 0.11 and External Quantum Efficiency up to 22.5%," Adv. Mater. **30**(12), 1705005 (2018).
33. K. Lee, J. Lee, E. Kim, J. Lee, D. Cho, J. Lim, D. Cho, J. Lim, C. Joo, J. Kim, S. Yoo, B. Ju, and J. Moon, "Simultaneously enhanced device efficiency, stabilized chromaticity of organic light emitting diodes with lambertian emission characteristic by random convex lenses," Nanotechnology **27**(7), 075202 (2016).
34. L. Deng, H. Zhou, S. Chen, H. Shi, B. Liu, L. Wang, and W. Huang, "Influence of wide-angle and multi-beam interference on the chromaticity and efficiency of top-emitting white organic light-emitting diodes," J. Appl. Phys. **117**(8), 083113 (2015).
35. M. K. Callens, D. Yokoyama, and K. Neyts, "Anisotropic materials in OLEDs for high outcoupling efficiency," Opt. Express **23**(16), 21128–21148 (2015).
36. D. Yokoyama, "Molecular orientation in small-molecule organic light-emitting diodes," J. Mater. Chem. **21**(48), 19187–19202 (2011).
37. C. Moon, S. Kim, J. Lee, and J. Kim, "Luminescence from oriented emitting dipoles in a birefringent medium," Opt. Express **23**(7), A279–A291 (2015).
38. R. Chance, A. Prock, and R. Silbey, "Molecular fluorescence and energy transfer near interfaces," Adv. Chem. Phys. **37**, 1–65 (1978).
39. K. Celebi, T. Heidel, and M. Baldo, "Simplified calculation of dipole energy transport in a multilayer stack using dyadic Green's functions," Opt. Express **15**(4), 1762–1772 (2007).
40. K. Kang, K. Y. Kim, and J. Kim, "Theoretical comparison of the excitation efficiency of waveguide and surface plasmon modes between quantum-mechanical and electromagnetic optical models of organic light-emitting diodes," Opt. Express **26**(22), A955–A973 (2018).
41. H. Cho, J. Chung, J. Song, J. Lee, H. Lee, J. Lee, J. Moon, S. Yoo, and N. S. Cho, "Importance of Purcell factor for optimizing structure of organic light-emitting diodes," Opt. Express **27**(8), 11057–11068 (2019).
42. Y. D. Zheng, F. A. Xiao, W. J. Liu, and X. L. Hu, "Purcell effect and light extraction of Tamm-plasmon-cavity green light-emitting diodes," Opt. Express **27**(21), 30852–30863 (2019).
43. X. Ke, H. Gu, X. Zhao, X. Chen, Y. Shi, C. Zhang, H. Jiang, and S. Liu, "Simulation method for study on outcoupling characteristics of stratified anisotropic OLEDs," Opt. Express **27**(16), A1014–A1029 (2019).
44. L. Penninck, P. Visschere, J. Beeckman, and K. Neyts, "Dipole radiation within one-dimensional anisotropic microcavities: a simulation method," Opt. Express **19**(19), 18558–18576 (2011).

Optics EXPRESS

45. H. Moon, B. Donderici, and F. Texeira, "Stable evaluation of Green's functions in cylindrically stratified regions with uniaxial anisotropic layers," J. Comput. Phys. **325**, 174–200 (2016).
46. M. Flämmich, D. Michaelis, and N. Danz, "Accessing OLED emitter properties by radiation pattern analyses," Org. Electron. **12**(1), 83–91 (2011).
47. J. L. Schnapf, T. W. Kraft, and D. A. Baylor, "Spectral sensitivity of human cone photoreceptors," Nature **325**(6103), 439–441 (1987).
48. International Commission on Illumination, "CIE 1931 color space," http://www.cie.co.at/.
49. X. Zhang, M. Trame, L. Lesko, and S. Schmidt, "Sobol Sensitivity Analysis: A Tool to Guide the Development and Evaluation of Systems Pharmacology Models," CPT: Pharmacometrics Syst. Pharmacol. **4**(2), 69–79 (2015).
50. Q. Ge and M. Menendez, "Extending Morris method for qualitative global sensitivity analysis of models with dependent inputs," Reliab. Eng. Syst. Safe. **162**, 28–39 (2017).
51. C. Kelley, *Iterative Method for Minimization* (Society for Industrial and Applied Mathematics, 1999).
52. J. Dobrowolski, "Versatile computer program for absorbing optical thin film systems," Appl. Opt. **20**(1), 74–81 (1981).
53. H. Gu, X. Chen, H. Jiang, C. Zhang, and S. Liu, "Optimal broadband Mueller matrix ellipsometer using multi-waveplates with flexibly oriented axes," J. Opt. **18**(2), 025702 (2016).
54. S. Liu, X. Chen, and C. Zhang, "Development of a broadband Mueller matrix ellipsometer as a powerful tool for nanostructure metrology," Thin Solid Films **584**, 176–185 (2015).
55. AG Fluxim, "Semiconducting emissive thin film optics simulator SETFOS," http://www.fluxim.com.